ELEMENTA
Science of the Anthropocene

Cho, C, et al. 2021. Evolution of formaldehyde (HCHO) in a plume originating from a petrochemical industry and its volatile organic compounds (VOCs) emission rate estimation. *Elem Sci Anth*, 9: 1. DOI: https://doi.org/10.1525/elementa.2021.00015

RESEARCH ARTICLE

Evolution of formaldehyde (HCHO) in a plume originating from a petrochemical industry and its volatile organic compounds (VOCs) emission rate estimation

Changmin Cho[1,2], Jason M. St. Clair[3,4], Jin Liao[3,5], Glenn M. Wolfe[3,4], Seokhan Jeong[1,6], Dae il Kang[7], Jinsoo Choi[8], Myung-Hwan Shin[8], Jinsoo Park[8], Jeong-Hoo Park[8], Alan Fried[9], Andrew Weinheimer[10], Donald R. Blake[11], Glenn S. Diskin[12], Kirk Ullmann[13], Samuel R. Hall[13], William H. Brune[14], Thomas F. Hanisco[3], and Kyung-Eun Min[1,*]

Large industrial facilities, such as petrochemical complexes, have decisive effects on regional air quality: directly due to their own hazardous volatile organic compounds (VOCs) emissions and indirectly due to their contribution to secondary air pollution. In South Korea, pronounced ozone and particulate matter issues have been reported in industrial areas. In this study, we develop a new top-down VOC emission rate estimation method using in situ airborne formaldehyde (HCHO) observations in the downwind plume of the Daesan Petrochemical Complex (DPC) in South Korea during the 2016 Korea–United States Air Quality (KORUS-AQ) mission. On May 22, we observed a peak HCHO mole fraction of 12 ppb after a transport time of 2.5 h (distance approximately 36 km) under conditions where the HCHO photochemical lifetime was 1.8 h. Box model calculations indicate that this elevated HCHO is mainly due to secondary production (more than 90% after 2 h of plume aging) from various VOC precursors including ethene, propene, and 1,3-butadiene. We estimate a lower limit for yearly DPC VOC emissions of 31 ($\pm$8.7) $\times$ 10^3 MT/year for HCHO precursors and 53 ($\pm$15) $\times$ 10^3 MT/year for all measured primary VOCs. These estimates are 1.5–2.5 times higher than the latest Korean emission inventories, KORUSv5. This method is beneficial not only by tracking the sources, sinks, and evolution of HCHO but also by validating existing emission inventories.

Keywords: Airborne HCHO measurement, VOCs emission rate estimation, Petrochemical industry, Top-down emission estimation, Emission inventory, VOCs emission in East Asia

1. Introduction

In the last few decades, there has been an increasing concern regarding anthropogenic volatile organic compounds (AVOCs) from industrial areas due to their carcinogenic characteristics and their role in O_3 and fine particle formation (Mazzuca et al., 2016; Seo et al., 2018),

[1] Atmospheric Trace Molecule Sensing Laboratory, School of Earth Sciences and Environmental Engineering, Gwangju Institute of Science and Technology, Gwangju, Republic of Korea

[2] Present affiliation: IEK-8: Troposphere, Institute of Energy and Climate Research, Forschungszentrum Jülich GmbH, Jülich, Germany

[3] Atmospheric Chemistry and Dynamics Lab, NASA Goddard Space Flight Center, Greenbelt, MD, USA

[4] Joint Center for Earth Systems Technology, University of Maryland Baltimore County, Baltimore, MD, USA

[5] Universities Space Research Association, Columbia, MD, USA

[6] Present affiliation: Environmental Assessment Group, Korea Environment Institute, Sejong, Republic of Korea

[7] Department of Atmospheric Engineering, National Institute of Environmental Research, Incheon, Republic of Korea

[8] Department of Air Quality, National Institute of Environmental Research, Incheon, Republic of Korea

[9] Institute of Arctic and Alpine Research (INSTAAR), University of Colorado, Boulder, CO, USA

[10] National Center for Atmospheric Research, Boulder, CO, USA

[11] Department of Chemistry, University of California Irvine, Irvine, CA, USA

[12] NASA Langley Research Center, Hampton, VA, USA

[13] Atmospheric Chemistry Observations & Modeling Laboratory, National Center for Atmospheric Research, Boulder, CO, USA

[14] Department of Meteorology, Pennsylvania State University, University Park, PA, USA

* Corresponding author:
Email: kemin@gist.ac.kr

especially in Asian countries due to their rapidly developing economies. For example, previous studies have reported air quality degradation in the highly polluted megacities and the densely concentrated industry complexes in Korea (Seo et al., 2014; Kim et al., 2017; Seo et al., 2018). To establish effective air pollution regulations, obtaining AVOC emission rates and speciation information from industrial areas is vital. However, in most Asian countries, such information is limited due to the lack of research resources and measurement opportunities.

Traditionally, there are two approaches to quantifying the VOC emission rate from a point source: bottom-up and top-down. Bottom-up inventories integrate all emission processes or sector-specific VOC emissions and are often done indirectly, relying on compiled emission factors (EFs), defined as the amount of gas and/or particle emission per unit activity or area. Due to the prohibitive cost of continuous and comprehensive VOC measurements, nationwide inventories are mainly compiled via this method. However, the VOCs emission inventories evaluated by this approach often have high variability among them and tend to be lower than those inferred from a top-down validation due to differences in EF depending on the calculation methods (Ryerson et al., 2003; Kim et al., 2011; Lee et al., 2011; Fang et al., 2016; Li et al., 2017). In particular, bottom-up approaches for large facilities like petrochemical plants often underestimate true emission rates because of the distributed nature of the sources and the resulting fugitive emissions (leakage from pipes, transmission lines, compressors, storage tanks, valves and fittings, etc.), which are difficult to quantify; Wert et al. (2003) demonstrated an order of magnitude underestimation of ethene and propene in bottom-up estimation compared to model derived values for Houston, Texas, petrochemical plumes.

A top-down approach estimates an emission rate using aircraft and/or satellite observations in combination with inverse modeling to infer the flux information from trace gas measurements (Stavrakou et al., 2009; Fang et al., 2016). The space-based implementation of this approach also has its limits: The number of VOCs observed from space is limited, and uncertainties associated with satellite retrievals limit accurate estimation in VOC emission strength (Tang et al., 2013). A mass balance approach with airborne measurements can also be used to quantify the emissions from point sources (White, 1976; Cambaliza et al., 2014; Peischl et al., 2015). In fact, a recent study done by Fried et al. (2020) employed this method (for the same facility in this study). However, as discussed in that paper, this method requires corrected and/or uncorrected time-resolved airborne observations of discrete but full coverage of speciated VOCs, as well as continuous high time resolution VOCs to ensure complete plume sampling. In addition, accurate mixed layer height determination and proof that the captured emissions fill the entire boundary layer are necessary.

As a complementary approach to ease off the requirements above, formaldehyde (HCHO) can be used since it is an indicator of parent VOC emission due to its high product yields from oxidation of VOCs (Bauwens et al., 2016; Wolfe et al., 2016a). Previous studies have shown that observations of HCHO can provide constraints on VOC emissions and their impact on air quality. de Gouw et al. (2015) showed an increasing HCHO mole fraction as a function of downwind distance from the third largest fuel ethanol refinery in the United States, suggesting that secondary HCHO production from VOC oxidation occurred in the plume. Hewitt et al. (2010) studied the photochemical processes of VOCs and resulting particle formation over a rainforest in Southeast Asia using fluorometric (Hantzsh reaction) HCHO measurements. Palmer et al. (2003) projected isoprene emissions over North America by utilizing satellite HCHO column observations. Moreover, ground-based HCHO measurements have been used to understand and improve upon knowledge of VOC sources and their loss pathways (Li et al., 2014; Zeng et al., 2015).

Taking advantage of the relationship between HCHO and its parent VOCs, in this study, we infer the amount of parent VOCs emissions from the observed HCHO mole fraction changes as HCHO forms in the downwind of the Daesan Petrochemical Complex (DPC) located on the Taean peninsula in South Korea at the edge of the Yellow Sea. Airborne in situ HCHO measurements of multiple plume crossings downwind, combined with a 0-D box model and information on the VOC speciation from the emitter, allows determination of HCHO production and loss terms in the plume and ultimately yields an estimate for the VOC emission rate from this source. A major motivation for this work is the release of the latest nationwide emission inventory of Korea, KORUSv5, which covers the emissions in Northeast Asia based on a bottom-up approach. The inventory covers East Asia by using the Sparse Matrix Operator Kernel Emissions (SMOKE-Asia; Woo et al., 2012) and SAPRC-99 chemical mechanism (Carter, 2000). The Korea–United-States Air Quality (KORUS-AQ) 2016 campaign provided the opportunity to validate this inventory via direct observations, which heretofore could not be validated by top-down measurements due to limitations in airborne VOC measurements. The approach for estimating VOC emission rates presented here can be performed without simultaneous comprehensive airborne VOC measurements, if the source signatures of various VOCs are given by emission inventory and/or ground measurements, enabling more frequent and lower cost validation of emission inventories for regional air quality improvement.

2. Methods

2.1. Data description

KORUS-AQ 2016 provided a valuable data set to investigate numerous contemporary air quality issues in South Korea. This mission was designed and conducted as an international cooperation between the United States and South Korea during May and June 2016. The KORUS-AQ effort was multi-platform and included aircraft (NASA DC-8, Hanseo University King Air, and NASA B200), ships (Onnuri and Jang Mok), ground sites (Mt. Taehwa, Olympic Park and 333 Korean air quality monitoring sites), satellite observations, and models to examine air quality characteristics in South Korea. Details about KORUS-AQ 2016,

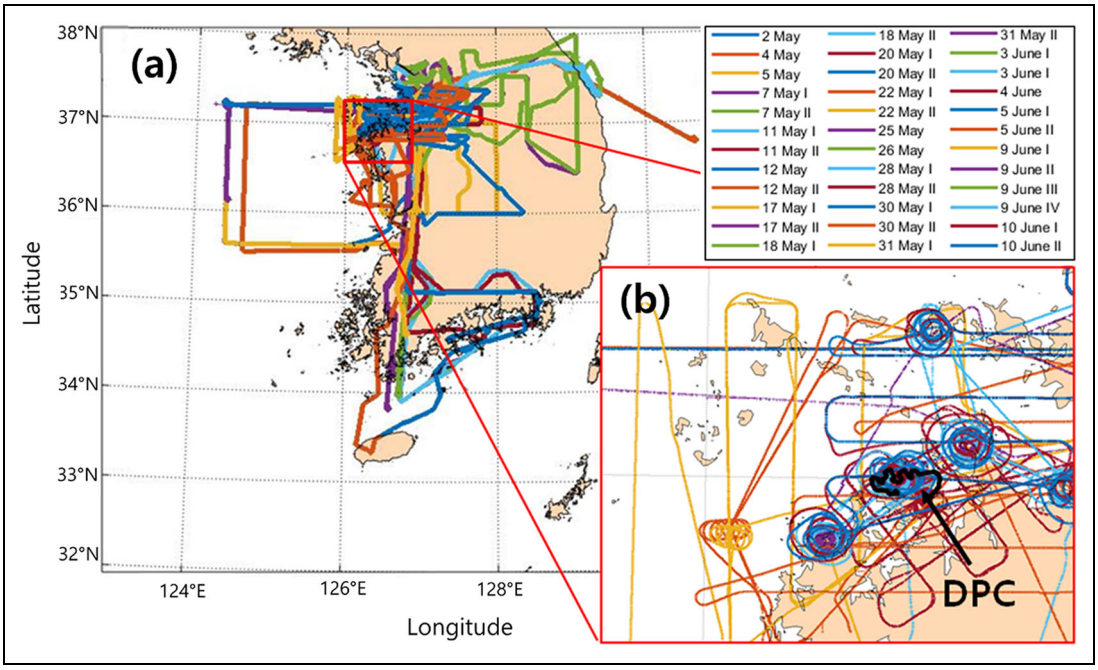

Figure 1. A map of Hanseo King Air flight tracks during KORUS-AQ 2016 for (a) all flights and (b) zoomed in near the Daesan Petrochemical Complex (DPC). Different color lines represent the individual flight tracks, and the thick black line represents the DPC area. DOI: https://doi.org/10.1525/elementa.2021.00015.f1

available data sets, and published scientific findings can be found at the project website (KORUS-AQ, 2021) and elsewhere (Miyazaki et al., 2018; Tang et al., 2018; Oak et al., 2019; Souri et al., 2020).

To validate the VOC emission inventory in South Korea, one of the key objectives of KORUS-AQ, many flights were specifically designed to survey the DPC. The DPC is ranked in the largest third of petrochemical facilities in South Korea and is located on the west coast of the Korean peninsula (**Figure 1**), where more than 70 petrochemical manufacturing facilities are located.

In this study, we focus on the analysis of HCHO measurements from the Hanseo King Air (HKA), since the lower airspeed and tighter turn radius of this aircraft allows for near-source sampling of large industrial facilities. A total 11 (**Figure 1b**) out of 36 research flights (**Figure 1a**) by the HKA included sampling in the vicinity of the DPC. The HKA sampled the source signatures of the DPC around various nearby power plants and various cities over the Taean peninsula. On May 22, the HKA flights (morning and afternoon) focused on sampling in the outflow of the DPC. The May 22 afternoon flight, shown in **Figure 2**, was the only successful flight able to sample a plume originating from the DPC with multiple aging stages, which is beneficial for investigating HCHO evolution and thus VOC emission strength estimation; the flight successfully captured the evolution of a plume from the DPC with 4 sampling crossings of the plume at similar altitude (320 $\pm$ 20 m above the sea level). This ideal sampling opportunity was due to favorable weather conditions with an easterly wind all day.

In situ HCHO measurements on HKA were conducted with the Compact Airborne Formaldehyde Experiment (CAFE) instrument built by NASA Goddard Space Flight

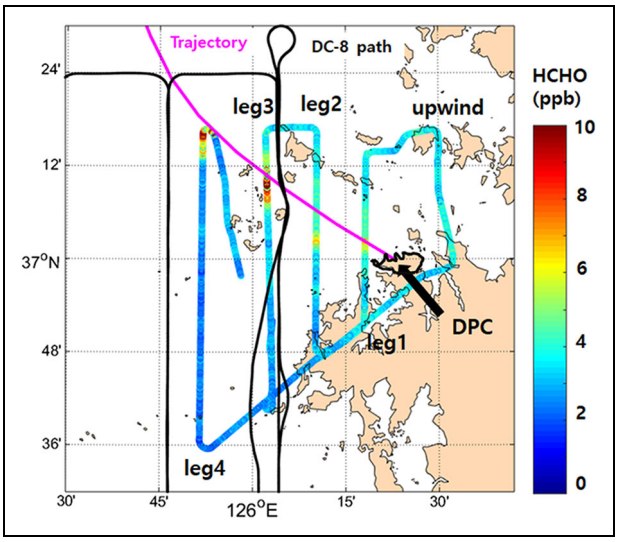

Figure 2. Mole fractions of formaldehyde (HCHO) downwind of the Daesan Petrochemical Complex (DPC) on May 22. The Hanseo King Air flight track is color-coded with HCHO mole fraction (ppb), and the magenta line indicates the forward trajectory of the air mass above the DPC using National Oceanic and Atmospheric Administration HYbrid Single-Particle Lagrangian Integrated Trajectory. The DC-8 flight path is indicated in black. The black arrow and the area surrounded by black curve indicate the location of the DPC. DOI: https://doi.org/10.1525/elementa.2021.00015.f2

Center. Details of the CAFE instrument and its Non-Resonant Laser Induced Fluorescence technique can be found elsewhere (St. Clair et al., 2017; St. Clair et al.,

2019). Briefly, HCHO molecules are excited by a moderate bandwidth, fixed wavelength laser at 355 nm. A fraction of excited HCHO molecules relax to the ground state with emission of fluorescence detected in the approximately 420–500 nm wavelength region. The calibration of CAFE was performed by adding flow (0–50 sccm, 1 sccm = 1 cm^3 min^{-1} at 1 atm and 25°C) from a HCHO cylinder (Air Liquide, preparation date: October 2012, 584 ppb HCHO in N_2) to the main flow, resulting in selectable HCHO mole fractions in the 0–10 ppb HCHO range (St. Clair et al., 2019). The HCHO cylinder was calibrated using Fourier-transform infrared spectroscopy before and after the campaign, and absolute uncertainty of the standard is 5%. By relating the observed fluorescence signal to calibration coefficients acquired in the laboratory, ambient HCHO abundance can be determined with a measurement uncertainty of $\pm 20\%$ with an offset uncertainty of $\pm$ 100 pptv. The 1σ precision at 1s integration time is 152 pptv (at HCHO = 0 pptv).

Other data sets used for this work are listed in Table 1. Details about species information as well as measurement technique and instrumental performance are provided. All the HKA data used in this study were time-synchronized before each research flight. DC-8 data were synchronized to the CO data as the common time basis before final data were submitted.

2.2. Model description

To estimate accurate VOC emissions by investigating the photochemical evolution of HCHO in the DPC plume, it is essential to separate primary and secondary HCHO sources in the observed plume. For that purpose, we use a box model, the Framework for 0-D Atmospheric Modeling (F0AM; Wolfe et al., 2016b), which enables the simulation of the photochemical evolution of Lagrangian plumes originating from a point source. The Master Chemical Mechanism v3.3.1 (Jenkin et al., 2015) is used for the near-explicit chemical oxidation mechanisms of VOCs and inorganics.

The May 22 HKA and DC-8 flights focused on sampling the chemical evolution of the DPC plume in the far-field outflow. Consequently, the initial mole fractions of all chemical species and photolysis frequencies in the model, depicting the near-field character of DPC emissions, were constrained with June 5 DC-8 observations close to the emissions source, as listed in Table S1 (see Section 3.2.3; Fried et al., 2020). To account for diluting effects of the constrained species, we apply first-order dilution with a rate coefficient of 1.3×10^{-5} s^{-1} calculated by the dispersion of CO (see Section 3.2.2). The background mole fractions of species in the model were taken from upwind sampling of the same flight which shows similar chemical conditions (NO_x: 3–5 ppbv, O_3: 60–80 ppb, CO: 270–300 ppb) as upwind sampling on the May 22 flight. With this F0AM model setting, the model ran for 2.5 h that correspond to the estimated plume evolution time (see Section 3.2.1). From the F0AM model, the secondary production rate of HCHO along the transect is extracted and compared with the inferred value from measurements.

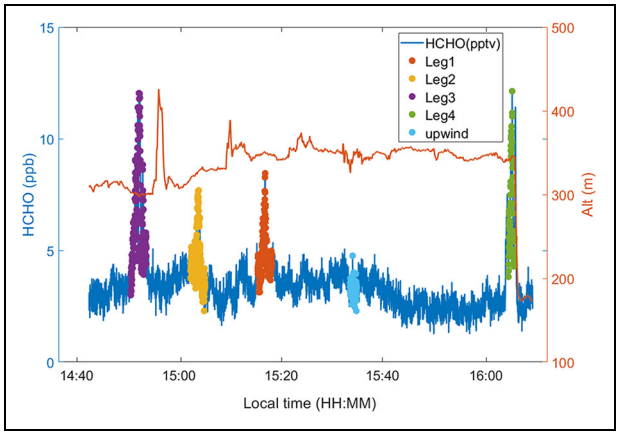

Figure 3. The time series of observed formaldehyde (HCHO) mole fraction (blue line) and altitude (red line) for the May 22 flight. Elevated HCHO mixing ratios in each leg are color-coded as orange, yellow, purple, and green referring to plume intersects from Leg1 to Leg4, respectively. The upwind baseline values are marked as light blue circles. DOI: https://doi.org/10.1525/elementa.2021.00015.f3

3. Estimation of VOCs emission rate from HCHO observation

3.1. Observed HCHO in DPC outflow

As mentioned in Section 2.1, the May 22 flight of the HKA was designed and successfully conducted to intercept the DPC plume several times (**Figure 2**). During the flight, elevated HCHO mole fractions in each leg were well captured by the measurements, as represented in **Figures 2** and **3**. A forward trajectory from the National Oceanic and Atmospheric Administration HYbrid Single-Particle Lagrangian Integrated Trajectory model (Stein et al., 2015) indicates that the HCHO enhanced air mass in each leg likely originated from the DPC, as represented by the magenta line in **Figure 2**. For convenience, each leg was named as Leg1–Leg4, with the leg number increasing with distance from the DPC. The time series of the observed HCHO mole fraction during the flight (**Figure 3**) shows high HCHO peaks of 8.5, 7.7, and 12.0 ppb for Leg1–Leg3, respectively. The HKA flight altitude (320 $\pm$ 20 m above sea level) and speed (75.5 $\pm$ 1.3 m/s) remained relatively constant except for Leg4, when the altitude decreased to 170 m when the HKA turned around. Time series of NO_2 and SO_2 (Figure S1) show peaks that coincide with HCHO in Legs 1, 2, and 3, while the peaks of HCHO, CO, NO_2, and SO_2 in Leg 4 overlapped with many structures, possibly indicating influence of other, non-DPC local sources. Thus, the observed HCHO in Leg 4 was excluded from further analysis.

3.2. HCHO mass balance

The differences in HCHO mole fraction between adjacent individual legs are the net balance of chemical production and loss processes, while the plume evolved from the former leg to the next adjacent leg, as shown in Equation 1 (Sumner et al., 2001). It is assumed that all HCHO enhancement in previous leg is transported to the next

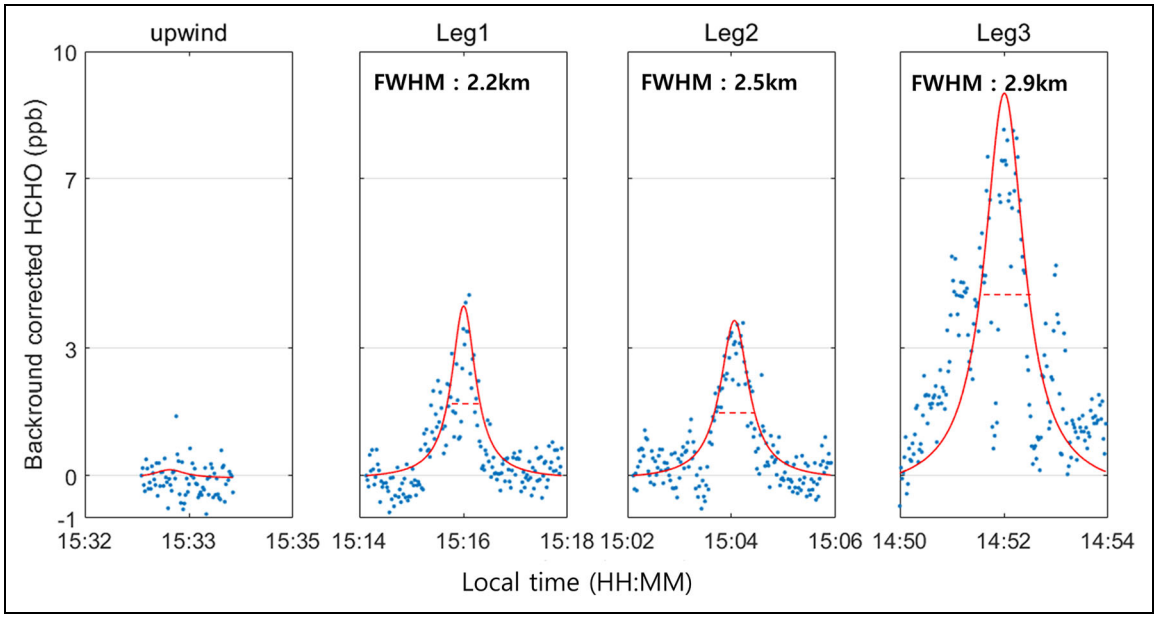

Figure 4. The formaldehyde (HCHO) enhancements in each leg and upwind from May 22 observations. The baseline-corrected HCHO mole fraction is represented as blue dots, and its Lorentzian curve fit is shown as red lines. Red dashed lines show the full width at half maximum (FWHM), and the values are on the upper part of each leg plot. DOI: https://doi.org/10.1525/elementa.2021.00015.f4

one within the time frame for the conservative estimation of secondary HCHO production.

$$\frac{\Delta C_{\mathrm{HCHO}}}{\Delta t} = P - L_{\mathrm{OH}} - L_{\mathrm{photolysis}} - L_{\mathrm{deposition}} - L_{\mathrm{dilution}} \,. \tag{1}$$

Here $\Delta C_{\mathrm{HCHO}}/\Delta t$ refers to the HCHO buildup rate, which describes HCHO mole fraction changes with respect to the air mass processing time. P is the secondary HCHO production rate from oxidation of VOCs. The L terms represent loss rates of HCHO by reaction with OH (L_{OH}), photolysis ($L_{\mathrm{photolysis}}$) and wet-, dry-deposition ($L_{\mathrm{deposition}}$), as well as dilution (L_{dilution}). The detailed procedures of quantifying each term in Equation 1 are described in following sections.

3.2.1. HCHO buildup rates

The buildup rates ($\Delta C_{\mathrm{HCHO}}/\Delta t$) can be quantified from the changes in HCHO abundance in each leg with respect to the reaction time. The elevated HCHO in the plume crossings are quantitatively assessed by integrating the enhanced HCHO along the plume width in each leg by using the Lorentzian fitted curve (which provides lower root mean square error (RMSE) than a Gaussian fit and expressed as in Equation 2) with subtracted baseline to account for background HCHO changes with time, as shown in **Figure 4**. The HCHO baselines in each leg were set to start the Lorentzian fitting with zero offset.

$$[\mathrm{HCHO}]_t = \frac{a}{\{(t-b)^2 + \mathrm{c}\}} + d \,. \tag{2}$$

Here, a, b, c, and d are fitting constants obtained from the Lorentzian fitting, and t represents the time when the plume was observed. Finally, from Equation 2, the fitted HCHO mole fractions ($[\mathrm{HCHO}]_t$) are obtained in each leg. The plume evolution times from the DPC to each leg were estimated as 0.5, 1.4, and 2.5 h, respectively, from the distance between the individual legs and the wind speed (4.3 ± 1.7 m/s) inferred from the average wind data from the DC-8 and a nearby ground meteorological site operated by Korea Meteorological Administration.

As a result, the inferred HCHO buildup rates are calculated as 2.5 (± 1.0) and 63.3 (± 28.5) ppt/s in between Leg1–Leg2 and Leg2–Leg3, respectively. Uncertainties in HCHO buildup rates (42%) are obtained from the Gaussian error propagation of HCHO measurement uncertainty (20%), uncertainty of wind speed (40% from its variability over the flight time as conservative estimation), and RMSE of Lorentzian fitting (12%, 13%, and 29% for individual errors from Leg1 to Leg3, respectively).

3.2.2. HCHO loss rates

HCHO in the plume is lost through several pathways, including oxidation, photolysis, deposition, and dilution. In this section, we describe procedures used to quantify the magnitude of each loss pathway.

Daytime HCHO removal by chemical reaction is governed by the OH radical (R1).

$$\mathrm{HCHO} + \mathrm{OH} \rightarrow \mathrm{H_2O} + \mathrm{HCO} \,. \tag{R1}$$

Therefore, the loss rate of HCHO by OH is calculated with Equation 3.

$$L_{\mathrm{OH}} = k_{\mathrm{HCHO+OH}} \times [\mathrm{HCHO}] \times [\mathrm{OH}]. \tag{3}$$

As described in Section 3.2.1, the enhancement of HCHO is inferred from the integrated area under the Lorentzian curve. The OH used in Equation 3 is estimated

Table 1. Instrumentation details for data used in this study. DOI: https://doi.org/10.1525/elementa.2021.00015.t1

Instrument (Method)	Payload	Measurement Species	Accuracy (1σ)	Reference
$NO_{xy}O_3$ (chemiluminescence with photolytic converter)	DC-8	NO	10%	Ridley and Grahek (1990)
		NO_2	10%	
		NO_y	20%	
		O_3	5%	
CAMS (mid-IR spectrometery)	DC-8	HCHO	3%	Richter et al. (2015)
ATHOS (laser-induced fluorescence)	DC-8	OH	32%	Faloona et al. (2004)
WAS (sampling canisters and gas chromatography)	DC-8	C_2-C_{10} VOCs	5% (20% for the oxygenated VOCs)	Blake et al. (2003)
DACOM (laser absorption spectrometer)	DC-8	CH_4	0.1%	Warner et al. (2010)
		CO	1%	
CAFS (actinic flux spectroradiometry)	DC-8	Photolysis frequencies	j_{HCHO}: 15%	Shetter and Müller (1999)
INS (internal navigation system)	DC-8	Meteorological parameters		–
CAFE (laser-induced fluorescence)	HKA	HCHO	20%	St. Clair et al. (2019); St. Clair et al. (2017)
SO_2 analyzer (Thermo 31i)	HKA	SO_2	1%	–
O_3 analyzer (Teledyne TAPI, T400)	HKA	O_3	0.5% above 100 ppb	–
NO_2 analyzer (Teledyne TAPI, T500U)	HKA	NO_2	0.5% above 5 ppb	–
CO analyzer (AeroLazer AL5002)	HKA	CO	3%	–

CAMS = Compact Airborne Multi-species Spectrometer; ATHOS = Airborne Tropospheric Hydrogen Oxides Sensor; WAS = Whole Air Sampler; DACOM = Differential Absorption Carbon monOxide Measurement; CAFS = Charged-coupled device Actinic Flux Spectroradiometers; CAFE = Compact Airborne Formaldehyde Experiment; VOC = volatile organic compound; HCHO = formaldehyde.

from DC-8-based observations by the Airborne Tropospheric Hydrogen Oxides Sensor (ATHOS) where the DC-8 sampled nearest to the HKA (as shown by the black line in **Figure 2**); the DC-8 flew at a similar altitude (approximately 300 m) but at a different overpass time (DC-8: approximately 11:00 KST, HKA: approximately 15:30 KST). Considering the time difference between the two flights, we scaled up the observed OH mixing ratio by 20%, based on the difference in photolysis frequencies of O_3 in corresponding time windows, which are estimated from the Tropospheric Ultraviolet and Visible Radiation Model v5.2 of National Center for Atmospheric Research (Madronich and Flocke, 1997). As a result, [OH] = 8.7 ($\pm$3.7) × 10^6 molecules/cm^3 was used for the HCHO chemical loss rate calculation with an uncertainty of 43% (20%, 20%, and 32% for uncertainties in reaction rate constant and measurement uncertainties of HCHO and OH, respectively).

The photolysis loss mechanism of HCHO is shown as R2 and R3 (Atkinson et al., 2004).

$$\mathrm{HCHO} + h\nu\ (< 324\ \mathrm{nm}) \rightarrow H_2 + \mathrm{CO} \qquad \text{(R2)}$$

$$\rightarrow \mathrm{H} + \mathrm{HCO} \qquad \text{(R3)}$$

The total photolysis loss rate of HCHO is calculated with Equation 4:

$$L_{\mathrm{Photolysis}} = (j_{\mathrm{HCHO}\rightarrow\mathrm{HCO+H}} + j_{\mathrm{HCHO}\rightarrow\mathrm{CO+H_2}}) \times [\mathrm{HCHO}], \qquad (4)$$

where j values are photolysis frequency (s^{-1}) of HCHO scaled up by 20% of the measured photolysis frequencies acquired by the Charged-coupled device Actinic Flux Spectroradiometers on the DC-8, in the same way OH was treated. Consequently, photolysis frequencies of R2 and R3 are 4.7 ($\pm$0.7) × 10^{-5} s^{-1} and 3.0 ($\pm$0.5) × 10^{-5} s^{-1}, respectively. Here, 15% errors were used for R2 and R3 photolysis rates as observational uncertainties (**Table 1**).

The depositional losses of HCHO are also considered under the assumption of a well-mixed boundary layer with no significant source(s) of HCHO near the surface. Here, we only include the dry depositional loss of HCHO since there was no precipitation on May 22. The loss rate of HCHO by dry deposition is calculated with Equation 5:

$$L_{\mathrm{deposition}} = \frac{V_d}{H} \times [\mathrm{HCHO}], \qquad (5)$$

where V_d is HCHO dry deposition velocity (cm/s) and H is planetary boundary layer (PBL) mixing height (km). We

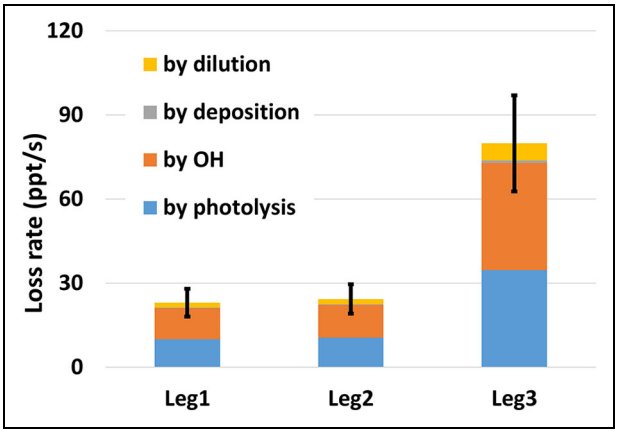

Figure 5. Estimated total loss rates of formaldehyde (HCHO) in each leg. Color bars represent the HCHO loss strength of dilution (yellow), deposition (gray), OH oxidation (orange), and photolysis (light blue). Vertical black bars denote the uncertainties propagated from the uncertainties of rate coefficients and measurements. DOI: https://doi.org/10.1525/elementa.2021.00015.f5

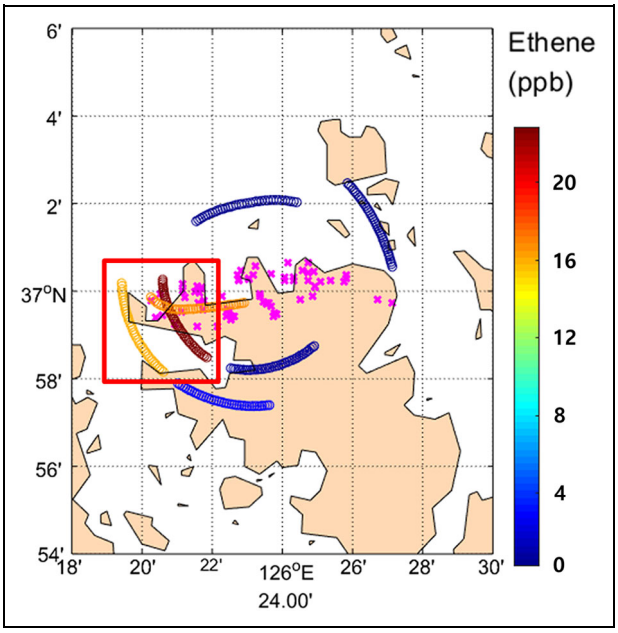

Figure 6. Measured ethene mole fractions from Whole Air Sampler on the DC-8 over the Daesan Petrochemical Complex (DPC) on June 5. Magenta X marks represent locations of stacks of the DPC petrochemical facilities. The red box represents the data used in this analysis. DOI: https://doi.org/10.1525/elementa.2021.00015.f6

estimate the PBL mixing height in this analysis as 1.7 ($\pm$0.2) km based on the vertical profile of temperature acquired from the profiling flight of the DC-8 on that day (Figure S2, which also confirms no significant changes in vertical mole fraction gradients among tracers, e.g., HCHO, CH_4 and benzene). We assume that the time difference between HKA (14:00–16:00, local time) and DC-8 profiling (10:00–12:00, local time) has a negligible influence on H, since both aircraft overpass times were in the middle of the day when the PBL is already fully developed. The V_d is taken from previous literature (0.25 $\pm$ 0.12 cm/s), which is directly measured over the water surface (Seyfioglu and Odabasi, 2006).

The mole fraction of HCHO in the plume is also reduced by dilution of the air mass along its trajectory. Hence, we considered the decrease in HCHO from dilution, with its rate calculated using Equation 6:

$$L_{\text{dilution}} = -\frac{d[\text{HCHO}]}{\text{dt}} = k_{\text{dil}}\left([\text{HCHO}] - [\text{HCHO}]_{\text{baseline}}\right). \quad (6)$$

The dilution rate constant of the plume (k_{dil}) is estimated as 1.3 ($\pm$0.2) $\times$ 10^{-5} s^{-1} using the decay rate of an unreactive chemical species (CO) measured on the DC-8 (Figure S3d). As a robustness test of our result, an alternative approach using the plume width was also employed to obtain an additional k_{dil} value using the observed HCHO plume broadening (more details in Section 4). For the uncertainty in k_{dil} estimation (22%), CO and wind measurement variability were used for conservative estimation.

Total loss rates can be calculated by summing all the individual loss processes described above as shown in **Figure 5**. The contributions of photolysis (48%) and oxidation by OH (43%) are the two major loss mechanisms of HCHO. Through this analysis, the HCHO lifetime is estimated as 1.8 h based on the total HCHO loss rate of 1.56 $\times$ 10^{-4} s^{-1} calculated using Equation 7.

$$k_{\text{HCHO}} = k_{\text{HCHO+OH}}[\text{OH}] + \text{j}_{\text{HCHO}\rightarrow\text{HCO+H}} + j_{\text{HCHO}\rightarrow\text{CO+H}_2} + \frac{V_d}{H} + k_{\text{dil}}.$$

This estimate falls in the range (1.5–2.5 h) of previously reported values (Dufour et al., 2009; Li et al., 2014; Kaiser et al., 2015). As a result, the total loss strengths of HCHO as the plume evolved are inferred as 23.6 ($\pm$6.2) and 52.1 ($\pm$13.5) ppt/s from Leg1 to Leg 2 and from Leg2 to Leg3, respectively. The uncertainty in the total HCHO loss rates is estimated as 26% from error propagation of individual loss processes.

3.2.3. Primary HCHO emission rates

The separation of primary and secondary contributions to the observed HCHO is necessary for quantifying the accurate VOCs emission rate from point sources, especially for giant emitters (e.g., petrochemical facilities) where a non-negligible amount of HCHO is directly emitted (Olaguer et al., 2009). In this section, we evaluate the significance of primary emissions to the HCHO enhancement observed in each leg. For this purpose, we used the model described in Section 2.2 to simulate the decay of HCHO primary emissions.

VOC speciation information for DPC emissions is essential for initializing the model. We use the VOC data set measured on June 5 by the DC-8 payload, primarily by the Whole Air Sampler (WAS), to represent the chemical speciation for the DPC plume. During the June 5 flight, the DC-8 circled around the DPC area to capture fresh emissions (approximately less than 7 min. of air processing time, Fried et al., 2020) from the DPC (as shown in **Figure 6**, color-

coded by ethene mole fraction). The wind direction during the flight was mainly northeasterly, thus the DC-8 was able to sample DPC emissions as a single outflow plume. Table S1 shows the chemical species used in this study and their average mole fractions as well as the initial conditions for our model run. We are assuming that the DPC VOC emissions speciation and rates did not drastically differ for the two sampling days—May 22 and June 5—since it is a large facility where yearly production lines operate as Fried et al. (2020) describe; VOC emission rates from the DPC on 3 different days during the mission are consistent within 23% from their mass balanced approach.

However, the relative fraction of captured VOCs mole fraction against the total VOC emission rate on those 2 days likely differs due to the difference in atmospheric stability and any offset of the sampling location with respect to the center of the plume. To reconcile the difference in degree of off-centered VOCs samples in two flights, we introduced a scaling factor (χ) for total VOC emission rate from the modeling estimation. Details related with χ can be found in Section 3.2.4.

Highly reactive VOCs (HRVOCs), such as ethene and propene as well as other VOCs as shown in Table S1, are major emitted species in the DPC and produce HCHO with high yield. For a conservative estimate in VOC emissions, we assume that HCHO observed over the DPC by the DC-8 is directly emitted from the stacks with minimal contribution from secondary HCHO; a sensitivity test of the possible contribution of secondary HCHO production is performed in Section 4. During the flight, high HCHO mole fractions up to 16 ppb (median: 10.3 ppb) were observed by Compact Airborne Multi-species Spectrometer over the DPC (Fried et al., 2020). Thus, the observed median HCHO mole fraction (10.3 ppb) over the DPC was considered as primary HCHO in the model, while the 2.7 ppb HCHO measured upwind (4 km from DPC) was set as model background. Due to the assumption of zero secondary HCHO contribution to the observed near-source HCHO in the conservative VOC emission rate estimate, the primary contribution of HCHO in the downwind area should be regarded as an upper limit.

To investigate the decay of primary HCHO further downwind of the DPC, 10.3 ppb of initial HCHO was tagged (HCHO′) with loss reactions of OH oxidation and photolysis with no secondary HCHO production from initial VOCs. **Figure 7** shows the HCHO mole fractions (HCHO and HCHO′) from the model simulation. As the plume evolves, the mole fraction of HCHO′ gradually decreases, and its mole fraction reaches background level (2.7 ppb, after 2.5 h of processing), while the HCHO mole fraction increases up to 17 ppb due to the secondary HCHO production from the oxidation of VOCs. In each Leg, the contributions of primary HCHO are 57%, 33%, and 7%, respectively.

As mentioned earlier, the absolute amount of VOCs in the plumes sampled from two different flights is not likely to be the same, so we only extracted the ratio of primary and secondary HCHO to the total HCHO enhancement in the model and then subtracted the contribution of the primary HCHO on the observed HCHO enhancement on

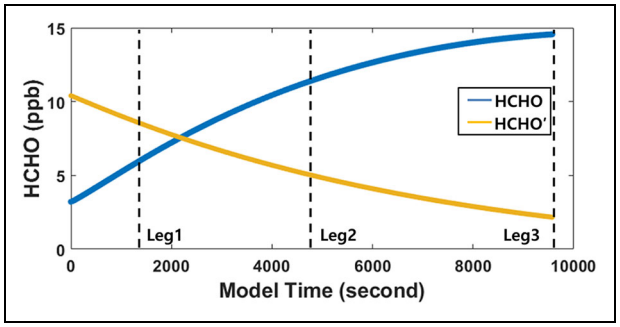

Figure 7. Model-estimated formaldehyde (HCHO; blue) and HCHO′ (orange) mole fraction time evolution. HCHO represents secondary HCHO formation, and HCHO′ shows the decay of primary HCHO. The black dashed lines represent the air mass processing time corresponding to the plume crossing in each leg. DOI: https://doi.org/10.1525/elementa.2021.00015.f7

the HKA May 22 flight to isolate the secondary HCHO contribution. The contributions of primary and secondary HCHO in the observed enhancement in each leg are shown in **Figure 8**. The primary HCHO contributes up to approximately 33% within 22 km (1.5 h of oxidation from DPC to Leg2) from the DPC. However, it significantly decreased (down to less than 7%) further downwind (2.6 h, after Leg3). This result is consistent with previous studies conducted at different chemical facilities; Jenkin et al. (2015) and Parrish et al. (2012) have shown that less than 10% of directly emitted HCHO survived 2–3 h downwind of emissions sources in the Houston Ship Channel. In addition, Fried et al. (2020) have estimated the upper limit contributions of the primary emission on HCHO production in the downwind of the DPC using the linear relationship between alkene-hydroxynitrate and HCHO (supplement). The primary contributions varied from 22% to 41% for the plume at different distances (21–44 km) and transit times (1.8–3.3 h) from the DPC to the plume sampling point (table S3 of Fried et al., 2020).

As a sensitivity test for the model prediction, the variability of HCHO production was tested by varying each initial constraint with its own uncertainty limit. The resulting 20% range in HCHO mole fraction was taken as the uncertainty for model estimation to be used for further error propagation.

3.2.4. Secondary HCHO production rates

Secondary HCHO production rates, $[P_{\mathrm{HCHO}}]_{\mathrm{inferred}}$, from the May 22 flight can be quantified as the net balance of HCHO buildup rates ($\frac{\Delta C_{\mathrm{HCHO}}}{\Delta t}$) and loss rates ($L_{\mathrm{Total}}$) as illustrated in Equation 8.

$$[P_{\mathrm{HCHO}}]_{\mathrm{inferred}} = \frac{\Delta C_{\mathrm{HCHO}}}{\Delta t} + L_{\mathrm{Total}}. \qquad (8)$$

Based on the estimations in previous sections, we inferred the secondary HCHO production rates as 35.0 ($\pm$8.7) ppt/s from Leg1 to Leg2, $[P_{\mathrm{HCHO},1\to2}]_{\mathrm{inferred}}$,

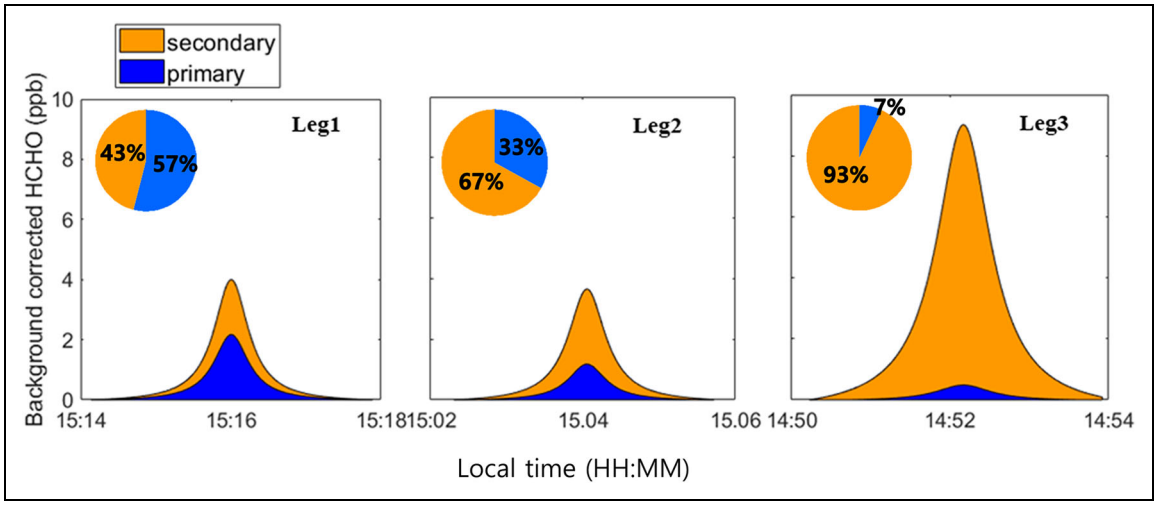

Figure 8. Primary and secondary formaldehyde (HCHO) contribution at each sampling leg as plume evolves. Blue (orange) areas are primary (secondary) HCHO. DOI: https://doi.org/10.1525/elementa.2021.00015.f8

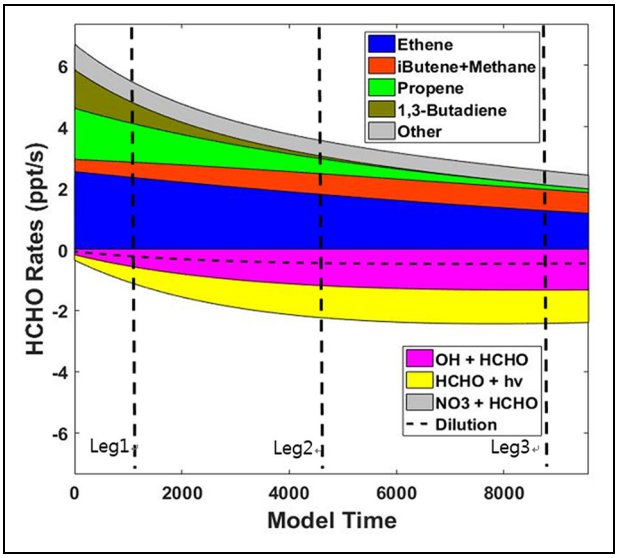

Figure 9. Box model results of instantaneous formaldehyde (HCHO) production and loss as the plume evolves. Horizontal dashed line represents reduction in HCHO by dilution, and vertical dashed lines represent the air mass processing time to match with plume crossings. DOI: https://doi.org/10.1525/elementa.2021.00015.f9

and 118.0 (±29.8) ppt/s from Leg2 to Leg3, $\left[P_{\mathrm{HCHO},2\to3}\right]_{\mathrm{inferred}}$.

Meanwhile, the model run provides secondary HCHO production rates as 4.5 (±0.9) ppt/s in between Leg1 and Leg2, $\left[P_{\mathrm{HCHO},1\to2}\right]_{\mathrm{model}}$, and 3.4 (±0.7) ppt/s in between Leg2 and Leg3, $\left[P_{\mathrm{HCHO},2\to3}\right]_{\mathrm{model}}$. The relative importance of VOC precursors evolves with time after the emission, as **Figure 9** demonstrates with the instantaneous HCHO production and loss rates as the plume evolves: HRVOCs like ethene, propene, and 1,3-butadiene are major precursors for secondary HCHO, but by Leg3 the fraction of HCHO originated from propene and 1,3-butadiene is small due to their relatively fast reaction with OH radicals. Methane and i-butane start to show their significance after 36 km downwind (2.5 h of plume evolving) due to their relatively slow oxidation rates.

The difference between secondary HCHO production rates from observation $\left[P_{\mathrm{HCHO},1\to2}\right]_{\mathrm{inferred}}$ and model $\left[P_{\mathrm{HCHO},1\to2}\right]_{\mathrm{model}}$ is likely due to the difference in the amount of VOCs inferred from May 22 by the HKA and June 5 as inequalities in atmospheric stability and sampling displacement from the center of the plume; errors in the model estimation of HCHO due to the uncertainties in chemical processes or the meteorological parameterization are canceled out since we take the difference in $[P_{\mathrm{HCHO}}]$ in adjacent legs. In addition, the discrepancy owing to unconstrained VOCs in our model due to the deficiency in measurements is not expected to be large as the calculated and measured OH reactivity right over DPC agrees well within their combined uncertainties. Thus, to reconcile the difference between the two secondary production rates, we introduced a scaling factor, χ (Equation 9) to account for the difference in the degree of the sampled air mass accounting for the entire plume on those two days.

$$\chi_{1\to2} = \frac{\left[P_{\mathrm{HCHO},1\to2}\right]_{\mathrm{measured}}}{\left[P_{\mathrm{HCHO},1\to2}\right]_{\mathrm{model}}} \quad \text{or } \chi_{2\to3} = \frac{\left[P_{\mathrm{HCHO},2\to3}\right]_{\mathrm{measured}}}{\left[P_{\mathrm{HCHO},2\to3}\right]_{\mathrm{model}}}. \tag{9}$$

The calculated χ are 7.8 (±2.5) from Leg1 to Leg2, $\chi_{1\to2}$ and 34.7 (±11.5) and from Leg2 to Leg3, $\chi_{2\to3}$, indicating that the inferred production rates from the observations are faster by 7.8 and 34.7 times than those in the model.

3.3. Estimation of VOC emission rates of the DPC

The near-source flight on June 5 provided a VOC emission source profile by sampling the direct emission over DPC. However, as the sampling was done at a fixed altitude (300 m) under stratified weather conditions (Fried et al., 2020), the sampled VOC source profile needed to be scaled to the conditions of May 22 as discussed in Section

3.2.4 with the χ. Therefore, we estimate the VOC emission rate of the DPC via Equation 10:

$$\text{Emission rate} = \chi \cdot C_{\text{VOC}} \cdot Q_{\text{total}},$$

where χ is a scaling factor as obtained from the HCHO secondary production rates (Equation 9), C_{VOC} stands for total VOC mole fraction by summing the measured VOC mole fractions which produce HCHO (ethene, propene 1,3-butadiene, isoprene, toluene, benzene, acetaldehyde, i-butane, and n-butane) in their oxidation process from the observed VOC source profile during the June 5 flight, and Q_{total} represents the total air flow rate from DPC facilities to the atmosphere. From the TeleMetering System and self-measuring system of the flow rate of individual stacks classified as larger facilities, which fall in business type I, II, and III at the DPC, Q_{total} is obtained as 3.8 ($\pm$0.1) $\times$ 10^{10} MT/year with 1% accuracy; this total flow rate is based on the flow rates of 270 stacks in 17 factories in DPC. As a result, the estimated emission rates are calculated as 31 ($\pm$8.7) $\times$ 10^3 MT/year and 139 ($\pm$46) $\times$ 10^3 MT/year by implementing the $\chi_{1\rightarrow2}$ and $\chi_{2\rightarrow3}$, respectively.

The uncertainties of the inferred HCHO production rates are propagated as 30% by considering all the uncertainties of each term in Equation 1 through Gaussian error propagation.

The substantial difference between the two emission rates is likely due to HCHO enhancements in between Leg2 and Leg3 caused by ship plumes from busy ferry and cruise lines in the region, as shown in Figure S4; bimodal peaks of SO_2 in Figure S1 also support an idea of additional plume mixing in observed HCHO in Leg3. Fried et al. (2020) also showed the complexities in source signature of one particular Daesan plume over the Yellow Sea (table S3 and figure S14 of Fried et al., 2020). Several studies have reported enhanced HCHO from ship emissions along the cruise lines due to direct emission and secondary production of HCHO from VOCs (Marbach et al., 2009; Song et al., 2010). If the additional HCHO is directly emitted from ships, it would immediately influence radical chemistry and thus O_3 formation in the near-field area; therefore, air quality degradations are expected further downwind. Therefore, additional constraints are required to separate the portion of HCHO from DPC to the other emission sources nearby in the enhanced HCHO in Leg3. On the other hand, there is less concern regarding additional ship-origin primary and/or secondary HCHO contribution in between Leg1 and Leg2 due to their vicinity to the DPC without any ship tracks and island in between (Figure S4). Consequently, we limit our further discussion of HCHO evolution to Leg1 and Leg2.

If all primary VOC species measured by WAS as listed in Table S1 are included in C_{VOC} (Equation 10) under the assumption of similar emission sources between HCHO precursor VOCs and others, the VOC emission rate increases to 53 ($\pm$15) $\times$ 10^3 MT/year, which agrees well, within estimated uncertainties, with the recently reported estimation based on a mass balance method (61 [$\pm$14] $\times$ 10^3 MT/year) by Fried et al. (2020). A possible and likely the main low bias in our conservative evaluation is due to the underestimation in Q_{total}, as described in Section 4, as well as neglecting HCHO from fugitive VOCs emissions.

4. Sensitivity analysis and discussion

To evaluate how robust our VOC emission rate estimation is with respect to the changes in the dilution rate, OH mole fraction, and fraction of primary HCHO, sensitivity tests were performed in addition to the discussion of possible bias in Q_{total}estimation.

Horizontal broadness of the observed HCHO plumes in each leg is used as an alternate approach for estimating dilution rate L_{dilution}. **Figure 4** shows how observed HCHO plumes span in the horizontal direction for individual legs. The difference of full width at half maximum (FWHM) values (2.2, 2.5, and 2.9 km for Leg1, Leg2, and Leg3, respectively) is used to calculate the dilution rate ($k_{\text{dil}}^{'}$) within the PBL height:

$$k_{\text{dil}}^{'} = \frac{\text{FWHM}_{\text{Leg3}} - \text{FWHM}_{\text{Leg1}}}{\text{H}}. \qquad (11)$$

This results in 2 times higher L_{dilution}, 2.6 ($\pm$0.6) $\times$ 10^{-5} s^{-1} than the L_{dilution} from CO (1.3 $\pm$ 0.2 $\times$ 10^{-5} s^{-1}) used in Section 3.2.2. This fast dilution rate increases the VOC emission rate by 7% (33 ($\pm$9.3) $\times$ 10^3 MT/year).

Another sensitivity test was conducted to assess our VOC emission rate estimate by varying the OH concentration in the plume, which is useful in addressing a number of potential uncertainties: (1) The fraction of primary and secondary HCHO determined from the model will depend on OH concentration in the plume. Also, (2) the OH concentration and its lifetime are likely lower in the core of the plume where higher mole fractions of OH reaction partners (e.g., CO, NO_x, and VOCs) exist than at the edges. Moreover, (3) the possible errors in OH estimation could be due to the overpass time difference between the DC-8 and HKA aircraft as described in Section 3.2.2. The estimated VOC emission rate varies as 33 ($\pm$9.4), 35 ($\pm$10), and 37 ($\pm$11) $\times$ 10^3 MT/year by changing 20%, 50%, and 75% less than the original scaled OH values, respectively. All the cases with OH-suppressing conditions inside of the plume result in higher VOC emission rates (7%, 15%, and 20%, respectively) than what we predicted as a conservative lower limit.

Furthermore, we tested the possible contribution of secondary HCHO production to the observed HCHO mole fraction on the June 5 DC-8 flight, which was assumed to be only direct HCHO emission from the DPC. Fried et al. (2020) found that up to 50% (upper limit estimation) of the observed HCHO on June 5 could be secondary. Therefore, the model was rerun with 50% of the initial HCHO (10.3 ppb), resulting in lower contributions of primary HCHO as 40%, 20%, and 4% from Leg1 to Leg3, respectively. The inferred HCHO secondary production rate was also lower as 32.8 ppt/s between Leg1 and Leg2. Finally, these changes in the primary HCHO contributions lead to a VOC emission rate of 33 ($\pm$9.5) $\times$ 10^3 MT/year (7% increase from the original estimation).

In addition, we only account for Q_{total} from the large plant facilities (only for business types I, II, and III) as described in Section 4. The estimated Q_{total} may be low

since more than 30 factories (business types IV and V or unclassified) exist in DPC and are not included in this analysis. Moreover, our method only infers HCHO from stacks, which is not likely the case in the real atmosphere where fugitive emissions of VOCs and thus their oxidation paths are not negligible.

Thus, one should note that our newly developed method only provides a lower limit on the VOC emission rate (HCHO precursor only) of the DPC ($31 \pm 8.8 \times 10^3$ MT/year), which is still 21.5 times higher than the KORUSv5 (21×10^3 MT/year of DPC VOCs), which will be even larger (up to a factor of 2.5) if we consider all measured VOC species ($53 \pm 15 \times 10^3$ MT/year). The discrepancy may indicate missing VOC sources in the inventory such as leaks/fugitive emissions from storage and/or emissions from smaller industrial facilities that are not regulated in Korea, in addition to possible biases in EFs of the various VOC emission activities in petrochemical processing; an order of magnitude higher or even larger fugitive VOC emissions than those in emission inventories have been independently reported by Wu et al. (2014) and (Chambers et al., 2008) from a Taiwan petrochemical tank farm and from Canadian refinery works, respectively. More efforts tracking fugitive emission sources together with their emission characteristics would help to reconcile the gap.

The large enhancement of secondary HCHO from oxidation of VOC emitted from DPC in the far downwind area (approximately 36 km) indicates a significant impact on regional air quality and health, including O_3 and particulate matter exposure. Direct toxicity of HCHO in the downwind area of DPC is a concern, as suggested by the Texas Commission on Environmental Quality (2008) report, which showed that long-term exposure of 3–15 ppb HCHO can cause respiratory symptoms and eye, nose, and throat irritation. As the current regional air quality models underestimate the actual emission inventory, they likely also underestimate the concerns of long-term exposure of HCHO.

5. Conclusions

It is essential to know accurate VOC emission strengths from various point sources for executing proper air pollution regulations. In this study, we described a new top-down estimation method developed to quantify the VOC emission rate of a large point source using in situ airborne HCHO observations. We used data from KORUS-AQ 2016 for this analysis, primarily the May 22 HKA flight. Several high peaks of HCHO (up to 12 ppb) were observed in the plume downwind of the DPC. HCHO increased at a rate of 2.5 ppt/s between the first and second legs and 63.3 ppt/s between the second and third legs. This sudden buildup of HCHO between the second and third legs is speculated as contribution from primary/secondary HCHO sources unrelated to the DPC, likely ship emissions. HCHO loss by OH and photolysis play a dominant role in HCHO removal, and the calculated HCHO lifetime was 1.8 h downwind of the petrochemical complex area in daytime. The contribution of HCHO primary emissions from the DPC to the observed HCHO enhancement is not significant in the far downwind region (<5% of observed HCHO after 2.6 h of daytime oxidation). The secondary HCHO production rate from DPC emissions is quantified as 35.4 ppt/s in between the first and second legs.

From the secondary HCHO production rates, we estimate a lower limit VOC emission rate from the DPC as 31 ($\pm$8.7) $\times$ 10^3 MT/year when only including HCHO precursor VOCs to 53 ($\pm$15) $\times$ 10^3 MT/year including all measured primary VOCs, which is 150%–250% of the existing inventory, KORUSv5. Our estimated VOC emission rate agrees with the recent work done by Fried et al. (2020) for the same facility via mass balance approach, and this strongly indicates a missing VOC source(s) even in the latest emission inventory. The discrepancy may be an indication of significant missing fugitive emissions as well as possible biases in EF determination for petrochemical production processes. Our newly developed top-down method utilizing fast airborne in situ measurements of HCHO demonstrates the viability of validating VOC point source emission rates with a limited set of VOC measurements and prior information on VOC speciation. This approach allows for more frequent inventory validation using lower cost small aircraft, ultimately developing more accurate VOC emission inventories and thus improving the cost-effectiveness of air pollution regulatory policies.

Data accessibility statement

All data used from the KORUS-AQ, including the DC-8 and HKA data, can be found at http://doi.org/10.5067/Suborbital/KORUSAQ/DATA01. The F0AM box model is available at https://github.com/AirChem/F0AM.

Supplemental files

The supplemental files for this article can be found as follows:

Table S1. Chemical species and their initial mole fractions for the box model, constrained by observations from the June 5 DC-8 flight.

Figure S1. The time series of observed HCHO, CO, NO_2, and SO_2 mole fractions during the May 22 flight of Hanseo King Air in the outflow of DPC.

Figure S2. Vertical profile of temperature, benzene, HCHO, and CH_4 from DC-8.

Figure S3. The measurements of OH, $J_{HCHO}\rightarrow H_2+CO$, $J_{HCHO}\rightarrow H+HCO$, and CO from the May 22 DC-8 flight.

Figure S4. Map of the DPC and downwind area with commercial ferry and cruise routes.

Acknowledgments

We thank the crew and science team of the campaign of KORUS-AQ for supporting the field campaign.

Funding

This research was supported by Technology Development Program to Solve Climate Changes through the National Research Foundation of Korea (NRF) funded by the Ministry of Science, ICT (NRF2019M1A2A2103953). Work by GSFC personnel was supported by the NASA Tropospheric Composition Program.

Competing interests

The authors declare that they have no conflict of interest.

Author contributions

Contributed to conception and design: K-EM, JHP, CCM.

Contributed to acquisition of data: CCM, JMC, JL, GMW, DIK, JSC, MHS, JSP, AF, AW, DRB, GSD, KU, SRH, WHB, TFH, K-EM.

Contributed to analysis and interpretation of data: K-EM, CCM.

Drafted and/or revised the article: K-EM, CCM, JSC.

References

Atkinson, R, Baulch, DL, Cox, RA, Crowley, JN, Hampson RF, Hynes, RG, Jenkin, ME, Rossi, MJ, Troe, J. 2004. IUPAC subcommittee for gas kinetic data evaluation. *Atmospheric Chemistry and Physics* **4**: 1461.

Bauwens, M, Stavrakou, T, Müller, JF, De Smedt, I, Van Roozendael, M, Werf, GR, Wiedinmyer, C, Kaiser, JW, Sindelarova, K, Guenther, A. 2016. Nine years of global hydrocarbon emissions based on source inversion of OMI formaldehyde observations. *Atmospheric Chemistry and Physics* **16**(15): 10133–10158. DOI: http://dx.doi.org/10.5194/acp-16-10133-2016.

Blake, NJ, Blake, DR, Simpson, IJ, Meinardi, S, Swanson, AL, Lopez, JP, Katzenstein, AS, Barletta, B, Shirai, T, Atlas, E, Sachse, G. 2003. NMHCs and halocarbons in Asian continental outflow during the Transport and Chemical Evolution over the Pacific (TRACE-P) field campaign: Comparison with PEM-West B. *Journal of Geophysical Research: Atmospheres* **108**(D20). DOI: http://dx.doi.org/10.1029/2002JD003367.

Cambaliza, MOL, Shepson, PB, Caulton, DR, Stirm, B, Samarov, D, Gurney, KR, Turnbull, J, Davis, KJ, Possolo, A, Karion, A, Sweeney, C. 2014. Assessment of uncertainties of an aircraft-based mass balance approach for quantifying urban greenhouse gas emissions. *Atmospheric Chemistry and Physics* **14**(17): 9029–9050. DOI: http://dx.doi.org/10.5194/acp-14-9029-2014.

Carter, WPL. 2000. Documentation of the SAPRC-99 Chemical Mechanism for VOC Reactivity Assessment, 92–329 and 95–308. Report to the California Air Resources Board, Contracts. Available at http://www.cert.ucr.edu/~carter/reactdat.htm.

Chambers, AK, Strosher, M, Wootton, T, Moncrieff, J, McCready, P. 2008. Direct measurement of fugitive emissions of hydrocarbons from a refinery. *Journal of the Air & Waste Management Association* **58**(8): 1047–1056. DOI: http://dx.doi.org/10.3155/1047-3289.58.8.1047.

de Gouw, JA, McKeen, SA, Aikin, KC, Brock, CA, Brown, SS, Gilman, JB, Graus, M, Hanisco, T, Holloway, JS, Kaiser, J, Keutsch, FN. 2015. Airborne measurements of the atmospheric emissions from a fuel ethanol refinery. *Journal of Geophysical Research: Atmospheres* **120**(9): 4385–4397. DOI: http://dx.doi.org/10.1002/2015JD023138.

Dufour, G, Wittrock, F, Camredon, M, Beekmann, M, Richter, A, Aumont, B, Burrows, JP. 2009. SCIAMACHY formaldehyde observations: Constraint for isoprene emission estimates over Europe? *Atmospheric Chemistry and Physics* **9**(5): 1647–1664. DOI: http://dx.doi.org/10.5194/acp-9-1647-2009.

Faloona, IC, Tan, D, Lesher, RL, Hazen, NL, Frame, CL, Simpas, JB, Harder, H, Martinez, M, Di Carlo, P, Ren, X, Brune, WH. 2004. A laser-induced fluorescence instrument for detecting tropospheric OH and HO2: Characteristics and calibration. *Journal of Atmospheric Chemistry* **47**(2): 139–167. DOI: http://dx.doi.org/10.1023/B:JOCH.0000021036.53185.0e.

Fang, X, Shao, M, Stohl, A, Zhang, Q, Zheng, J, Guo, H, Wang, C, Wang, M, Ou, J, Thompson, RL, Prinn, RG. 2016. Top-down estimates of benzene and toluene emissions in the Pearl River Delta and Hong Kong, China. *Atmospheric Chemistry and Physics* **16**(5): 3369–3382. DOI: http://dx.doi.org/10.5194/acp-16-3369-2016.

Fried, A, Walega, J, Weibring, P, Richter, D, Simpson, IJ, Blake, DR, Blake, NJ, Meinardi, S, Barletta, B, Hughes, SC, Crawford, JH. 2020. Airborne formaldehyde and VOC measurements over the Daesan petrochemical complex on Korea's northwest coast during the KORUS-AQ study: estimation of emission fluxes and effects on air quality. *Elementa: Science of the Anthropocene* **8**(1). DOI: https://doi.org/10.1525/elementa.2020.121.

Hewitt, CN, Lee, JD, MacKenzie, AR, Barkley, MP, Carslaw, N, Carver, GD, Chappell, NA, Coe, H, Collier, C, Commane, R, Davies, F. 2010. Overview: Oxidant and particle photochemical processes above a south-east Asian tropical rainforest (the OP3 project): introduction, rationale, location characteristics and tools. *Atmospheric Chemistry and Physics* **10**(1): 169–199. DOI: http://dx.doi.org/10.5194/acp-10-169-2010.

Jenkin, ME, Young, JC, Rickard, AR. 2015. The MCM v3.3.1 degradation scheme for isoprene. *Atmospheric Chemistry and Physics* **15**(20): 11433–11459. DOI: http://dx.doi.org/10.5194/acp-15-11433-2015.

Kaiser, J, Wolfe, GM, Min, KE, Brown, SS, Miller, CC, Jacob, DJ, DeGouw, JA, Graus, M, Hanisco, TF, Holloway, J, Peischl, J. 2015. Reassessing the ratio of glyoxal to formaldehyde as an indicator of hydrocarbon precursor speciation. *Atmospheric Chemistry and Physics* **15**(13): 7571–7583. DOI: http://dx.doi.org/10.5194/acp-15-7571-2015.

Kim, HC, Kim, S, Kim, B-U, Jin, C-S, Hong, S, Park, R, Son, SW, Bae, C, Bae, M, Song, CK, Stein, A. 2017. Recent increase of surface particulate matter concentrations in the Seoul Metropolitan Area, Korea. *Scientific Reports* **7**(1): 4710. DOI: http://dx.doi.org/10.1038/s41598-017-05092-8.

Kim, SW, McKeen, SA, Frost, GJ, Lee, SH, Trainer, M, Richter, A, Angevine, WM, Atlas, E, Bianco, L, Boersma, KF, Brioude, J. 2011. Evaluations of NOx and highly reactive VOC emission inventories in Texas and their implications for ozone plume simulations during the Texas Air Quality Study 2006. *Atmospheric Chemistry and Physics* **11**(22): 11361–

11386. DOI: http://dx.doi.org/10.5194/acp-11-11361-2011.

KORUS-AQ. 2021. Available at https://espo.nasa.gov/korus-aq.

Lee, DG, Lee, YM, Jang, KW, Yoo, C, Kang, K. H, Lee, JH, Jung, SW, Park, JM, Lee, SB, Han, JS, Hong, JH, Lee, SJ. 2011. Korean national emissions inventory system and 2007 air pollutant emissions. *Asian Journal of atmospheric environment* **5**(4): 278–291. DOI: http://dx.doi.org/10.5572/ajae.2011.5.4.278.

Li, S-M, Leithead, A, Moussa, SG, Liggio, J, Moran, MD, Wang, D, Hayden, K, Darlington, A, Gordon, M, Staebler, R, Makar, PA. 2017. Differences between measured and reported volatile organic compound emissions from oil sands facilities in Alberta, Canada. *Proceedings of the National Academy of Sciences of the United States of America* **114**(19): E3756–E3765. DOI: http://dx.doi.org/10.1073/pnas.1617862114.

Li, X, Rohrer, F, Brauers, T, Hofzumahaus, A, Lu, K, Shao, M, Zhang, YH, Wahner, A. 2014. Modeling of HCHO and CHOCHO at a semi-rural site in southern China during the PRIDE-PRD2006 campaign. *Atmospheric Chemistry and Physics* **14**(22): 12291–12305. DOI: http://dx.doi.org/10.5194/acp-14-12291-2014.

Madronich, S, Flocke, S. 1997. Theoretical estimation of biologically effective UV radiation at the Earth's surface, in Zerefos, CS, Bais, AF eds., *Solar ultraviolet radiation: Modelling, measurements and effects*. Berlin, Heidelberg: Springer: 23–48.

Marbach, T, Beirle, S, Platt, U, Hoor, P, Wittrock, F, Richter, A, Vrekoussis, M, Grzegorski, M, Burrows, JP, Wagner, T. 2009. Satellite measurements of formaldehyde linked to shipping emissions. *Atmospheric Chemistry and Physics* **9**(21): 8223–8234. DOI: http://dx.doi.org/10.5194/acp-9-8223-2009.

Mazzuca, GM, Ren, X, Loughner, CP, Estes, M, Crawford, JH, Pickering, KE, Weinheimer, AJ, Dickerson, RR. 2016. Ozone production and its sensitivity to NOx and VOCs: Results from the DISCOVER-AQ field experiment, Houston 2013. *Atmospheric Chemistry and Physics* **16**(22): 14463–14474. DOI: http://dx.doi.org/10.5194/acp-16-14463-2016.

Miyazaki, K, Sekiya, T, Fu, DW, Bowman, KS, Kulawik, S, Sudo, K, Walker, T, Kanaya, Y, Takigawa, M, Ogochi, K, Eskes, H. 2018. Balance of emission and dynamical controls on ozone during KORUS-AQ from multi-constituent satellite data assimilation. *Journal of Geophysical Research: Atmospheres* **124**. DOI: http://dx.doi.org/10.1029/2018JD028912.

Oak, Y, Park, R, Schroeder, J, Crawford, J, Blake, D, Weinheimer, AJ, Woo, JH, Kim, SW, Yeo, H, Fried, A, Wisthaler, A. 2019. Evaluation of simulated O_3 production efficiency during the KORUS-AQ campaign: Implications for anthropogenic NO_X emissions in Korea. *Elementa: Science of the Anthropocene* **7**: 56. DOI: http://dx.doi.org/10.1525/elementa.394.

Olaguer, EP, Rappenglück, B, Lefer, B, Stutz, J, Dibb, J, Griffin, R, Brune, WH, Shauck, M, Buhr, M, Jeffries, H, Wiuete, W. 2009. Deciphering the role of radical precursors during the second Texas air quality study. *Journal of the Air & Waste Management Association* **59**(11): 1258–1277. DOI: http://dx.doi.org/10.3155/1047-3289.59.11.1258.

Palmer, PI, Jacob, DJ, Fiore, AM, Martin, RV, Chance, K, Kurosu, TP. 2003. Mapping isoprene emissions over North America using formaldehyde column observations from space. *Journal of Geophysical Research: Atmospheres* **108**(D6): n/a-n/a. DOI: http://dx.doi.org/10.1029/2002JD002153.

Parrish, DD, Ryerson, TB, Mellqvist, J, Johansson, J, Fried, A, Richter, D, Walega, JG, Washenfelder, RD, De Gouw, JA, Peischl, J, Aikin, KC. 2012. Primary and secondary sources of formaldehyde in urban atmospheres: Houston Texas region. *Atmospheric Chemistry and Physics* **12**(7): 3273–3288. DOI: http://dx.doi.org/10.5194/acp-12-3273-2012.

Peischl, J, Ryerson, TB, Aikin, KC, de Gouw, JA, Gilman, JB, Holloway, JS, Lerner, BM, Nadkarni, R, Neuman, JA, Nowak, JB, Trainer, M. 2015. Quantifying atmospheric methane emissions from the Haynesville, Fayetteville, and northeastern Marcellus shale gas production regions. *Journal of Geophysical Research: Atmospheres* **120**(5): 2119–2139. DOI: http://dx.doi.org/10.1002/2014JD022697.

Richter, D, Weibring, P, Walega, JG, Fried, A, Spuler, SM, Taubman, MS. 2015. Compact highly sensitive multi-species airborne mid-IR spectrometer. *Applied Physics B* **119**(1): 119–131. DOI: http://dx.doi.org/10.1007/s00340-015-6038-8.

Ridley, BA, Grahek, FE. 1990. A small, low flow, high sensitivity reaction vessel for NO chemiluminescence detectors. *Journal of Atmospheric and Oceanic Technology* **7**(2): 307–311. DOI: http://dx.doi.org/10.1175/1520-0426(1990)007<0307:Aslfhs>2.0.Co;2.

Ryerson, TB, Trainer, M, Angevine, WM, Brock, CA, Dissly, RW, Fehsenfeld, FC, Frost, GJ, Goldan, PD, Holloway, JS, Hübler, G, Jakoubek, RO. 2003. Effect of petrochemical industrial emissions of reactive alkenes and NO_X on tropospheric ozone formation in Houston, Texas. *Journal of Geophysical Research: Atmospheres* **108**(D8). DOI: http://dx.doi.org/10.1029/2002JD003070.

Seo, J, Park, DSR, Kim, JY, Youn, D, Lim, YB, Kim, Y. 2018. Effects of meteorology and emissions on urban air quality: A quantitative statistical approach to long-term records (1999–2016) in Seoul, South Korea. *Atmospheric Chemistry and Physics* **18**(21): 16121–16137. DOI: http://dx.doi.org/10.5194/acp-18-16121-2018.

Seo, J, Youn, D, Kim, JY, Lee, H. 2014. Extensive spatiotemporal analyses of surface ozone and related meteorological variables in South Korea for the

period 1999–2010. *Atmospheric Chemistry and Physics* **14**(12): 6395–6415. DOI: http://dx.doi.org/10.5194/acp-14-6395-2014.

Seyfioglu, R, Odabasi, M. 2006. Investigation of air–water exchange of formaldehyde using the water surface sampler: Flux enhancement due to chemical reaction. *Atmospheric Environment* **40**(19): 3503–3512. DOI: http://dx.doi.org/10.1016/j.atmosenv.2006.01.048.

Shetter, RE, Müller, M. 1999. Photolysis frequency measurements using actinic flux spectroradiometry during the PEM-Tropics mission: Instrumentation description and some results. *Journal of Geophysical Research: Atmospheres* **104**(D5): 5647–5661. DOI: http://dx.doi.org/10.1029/98JD01381.

Song, CH, Kim, HS, von Glasow, R, Brimblecombe, P, Kim, J, Park, RJ, Woo, JH, Kim, YH. 2010. Source identification and budget analysis on elevated levels of formaldehyde within the ship plumes: A ship-plume photochemical/dynamic model analysis. *Atmospheric Chemistry and Physics* **10**(23): 11969–11985. DOI: http://dx.doi.org/10.5194/acp-10-11969-2010.

Souri, AH, Nowlan, CR, González Abad, G, Zhu, L, Blake, DR, Fried, A, Weinheimer, AJ, Wisthaler, A, Woo, JH, Zhang, Q, Chan Miller, CE. 2020. An inversion of NO_X and non-methane volatile organic compound (NMVOC) emissions using satellite observations during the KORUS-AQ campaign and implications for surface ozone over East Asia. *Atmospheric Chemistry and Physics* **20**(16): 9837–9854. DOI: http://dx.doi.org/10.5194/acp-20-9837-2020.

Stavrakou, T, Müller, JF, De Smedt, I, Van Roozendael, M, Kanakidou, M, Vrekoussis, M, Wittrock, F, Richter, A, Burrows, JP. 2009. The continental source of glyoxal estimated by the synergistic use of spaceborne measurements and inverse modelling. *Atmospheric Chemistry and Physics* **9**(21): 8431–8446. DOI: http://dx.doi.org/10.5194/acp-9-8431-2009.

St. Clair, JM, Swanson, AK, Bailey, SA, Hanisco, TF. 2019. CAFE: A new, improved nonresonant laser-induced fluorescence instrument for airborne in situ measurement of formaldehyde. *Atmospheric Measurement Techniques* **12**(8): 4581–4590. DOI: http://dx.doi.org/10.5194/amt-12-4581-2019.

St. Clair, JM, Swanson, AK, Bailey, SA, Wolfe, GM, Marrero, JE, Iraci, LT, Hagopian, JG, Hanisco, TF. 2017. A new non-resonant laser-induced fluorescence instrument for the airborne in situ measurement of formaldehyde. *Atmospheric Measurement Techniques* **10**(12): 4833–4844. DOI: http://dx.doi.org/10.5194/amt-10-4833-2017.

Stein, AF, Draxler, RR, Rolph, GD, Stunder, BJB, Cohen, MD, Ngan, F. 2015. NOAA's HYSPLIT atmospheric transport and dispersion modeling system. *Bulletin of the American Meteorological Society* **96**(12): 2059–2077. DOI: http://dx.doi.org/10.1175/bams-d-14-00110.1.

Sumner, AL, Shepson, PB, Couch, TL, Thornberry, T, Carroll, MA, Sillman, S, Pippin, M, Bertman, S, Tan, D, Faloona, I, Brune, W. 2001. A study of formaldehyde chemistry above a forest canopy. *Journal of Geophysical Research: Atmospheres* **106**(D20): 24387–24405. DOI: http://dx.doi.org/10.1029/2000JD900761.

Tang, W, Arellano, AF, DiGangi, JP, Choi, Y, Diskin, GS, Agustí-Panareda, A, Parrington, M, Massart, S, Gaubert, B, Lee, Y, Kim, D. 2018. Evaluating high-resolution forecasts of atmospheric CO and CO_2 from a global prediction system during KORUS-AQ field campaign. *Atmospheric Chemistry and Physics* **18**(15): 11007–11030. DOI: http://dx.doi.org/10.5194/acp-18-11007-2018.

Tang, W, Cohan, DS, Lamsal, LN, Xiao, X, Zhou, W. 2013. Inverse modeling of Texas NO_X emissions using space-based and ground-based NO_2 observations. *Atmospheric Chemistry and Physics* **13**(21): 11005–11018. DOI: http://dx.doi.org/10.5194/acp-13-11005-2013.

Warner, JX, Wei, Z, Strow, LL, Barnet, CD, Sparling, LC, Diskin, G, Sachse, G. 2010. Improved agreement of AIRS tropospheric carbon monoxide products with other EOS sensors using optimal estimation retrievals. *Atmospheric Chemistry and Physics* **10**(19): 9521–9533. DOI: http://dx.doi.org/10.5194/acp-10-9521-2010.

Wert, BP, Trainer, M, Fried, A, Ryerson, TB, Henry, B, Potter, W, Angevine, WM, Atlas, E, Donnelly, SG, Fehsenfeld, FC, Frost, GJ. 2003. Signatures of terminal alkene oxidation in airborne formaldehyde measurements during TexAQS 2000. *Journal of Geophysical Research: Atmospheres* **108**(D3). DOI: http://dx.doi.org/10.1029/2002JD002502.

White, WH, Anderson, JA, Blumenthal, DL, Husar, RB, Gillani, NV, Husar, JD, Wilson, WE. 1976. Formation and transport of secondary air pollutants: Ozone and aerosols in the St. Louis urban plume. *Science* **194**: 187–189. DOI: http://dx.doi.org/10.1126/science.959846.

Wolfe, GM, Kaiser, J, Hanisco, TF, Keutsch, FN, de Gouw, JA, Gilman, JB, Graus, M, Hatch, CD, Holloway, J, Horowitz, LW, Lee, BH. 2016a. Formaldehyde production from isoprene oxidation across NO_X regimes. *Atmospheric Chemistry and Physics* **16**(4): 2597–2610. DOI: http://dx.doi.org/10.5194/acp-16-2597-2016.

Wolfe, GM, Marvin, MR, Roberts, SJ, Travis, KR, Liao, J. 2016b. The Framework for 0-D Atmospheric Modeling (F0AM) v3.1. *Geoscientific Model Development* **9**(9): 3309–3319. DOI: http://dx.doi.org/10.5194/gmd-9-3309-2016.

Woo, J-H, Choi, K-C, Kim, HK, Baek, BH, Jang, M, Eum, J-H, Song, CH, Ma, Y-I, Sunwoo, Y, Chang, L-S, Yoo, SH. 2012. Development of an anthropogenic emissions processing system for Asia using SMOKE. *Atmospheric Environment* **58**: 5–13. DOI: http://dx.doi.org/10.1016/j.atmosenv.2011.10.042.

Wu, C-F, Wu, T-g, Hashmonay, RA, Chang, S-Y, Wu, Y-S, Chao, CP, Hsu, CP, Chase, MJ, Kagann, RH. 2014. Measurement of fugitive volatile organic compound emissions from a petrochemical tank farm using open-path Fourier transform infrared spectrometry. *Atmospheric Environment* **82**: 335–342. DOI: http://dx.doi.org/10.1016/j.atmosenv.2013.10.036.

Zeng, G, Williams, JE, Fisher, JA, Emmons, LK, Jones, NB, Morgenstern, O, Robinson, J, Smale, D, Paton-Walsh, C, Griffith, DW. 2015. Multi-model simulation of CO and HCHO in the Southern Hemisphere: Comparison with observations and impact of biogenic emissions. *Atmospheric Chemistry and Physics* **15**(13): 7217–7245. DOI: http://dx.doi.org/10.5194/acp-15-7217-2015.

How to cite this article: Cho, C, St. Clair, JM, Liao, J, Wolfe, GM, Jeong, S, Kang, DI, Choi, J, Shin, M-H, Park, J, Park, J-H, Fried, A, Weinheimer, A, Blake, DR, Diskin, GS, Ullmann, K, Hall, SR, Brune, WH, Hanisco, TF, Min, K-E. 2021. Evolution of formaldehyde (HCHO) in a plume originating from a petrochemical industry and its volatile organic compounds (VOCs) emission rate estimation. *Elementa: Science of the Anthropocene* 9(1). DOI: https://doi.org/10.1525/elementa.2021.00015

Domain Editor-in-Chief: Detlev Helmig, Boulder AIR LLC, Boulder, CO, USA

Associate Editor: Alex Guenther, Department of Earth System Science, University of California, Irvine, CA, USA

Knowledge Domain: Atmospheric Science

Part of an Elementa Special Feature: KORUS-AQ

Published: August 4, 2021 **Accepted:** June 29, 2021 **Submitted:** February 25, 2021

ELEMENTA Science of the Anthropocene

Elem Sci Anth is a peer-reviewed open access journal published by University of California Press.

OPEN ACCESS